Numerical Simulation of Micropolar Flow in a Channel under Oscillatory Pressure Gradient

Ashraf, Muhammad*+

Centre for Advanced Studies in Pure and Applied Mathematics, Bahauddin Zakariya University, Multan, PAKISTAN

Ali, Kashif

Department of Basic Sciences and Humanities, Muhammad Nawaz Sharif University of Engineering and Technology, Multan, PAKISTAN

Ashraf, Muhammad*+

Centre for Advanced Studies in Pure and Applied Mathematics, Bahauddin Zakariya University, Multan, PAKISTAN

ABSTRACT: *We numerically investigate the pulsatile flow and heat transfer of a micropolar fluid through a Darcy-Forchhmeir porous channel in the presence of wall transpiration. We use the central difference approximations for the spatial derivatives, whereas the time integration has been performed by employing the three steps explicit Runge-Kutta method to obtain the numerical solution. It is noted that the Darcy parameter tends to accelerate the fluid, whereas the Forchheimer quadratic drag parameter and the magnetic parameter would reduce the flow velocity. The effect of the steady component of the pressure gradient is to remarkably accelerate the flow whereas that of the oscillatory component is time-dependent. An increase in the Prandtl number tends to almost straighten the temperature profiles.*

KEYWORDS: *Pulsatile flow, Darcy-Forchhmeir model; Micropolar fluid; Three-step explicit R.K. method.*

INTRODUCTION

Fluids having non-Newtonian nature have been studied for many decades as they are important in the industry. Because of the complex nature of these fluids, numerous models are proposed but the micropolar model is quite famous. In different geometries, the micropolar flows have been studied by many researchers. For example, *Fakour et al.* [1] analytically investigated the micropolar fluid flow in a channel subject to a chemical reaction using the Least Square Method (LSM). The results revealed that the LSM could achieve suitable results in predicting the solutions of such problems. The study further showed that the stream function decreased with the increase in the Reynolds number. Effects of chemical reaction, thermal stratification, Soret and Dufour numbers on magneto-hydrodynamic free convective heat and mass transfer of a viscous, incompressible, and electrically conducting fluid on a vertical stretching surface embedded in a saturated porous medium were presented by *Mehrabian et al.* [2]. A similarity transform was used to reduce the governing partial differential equations into a system of nonlinear ordinary differential equations, solved by an analytical method which led to an expression acceptable for all values of the effective parameters. The study of steady laminar natural convective flow and heat transfer of

* *To whom correspondence should be addressed.*
+ E-mail: mashraf_mul@yahoo.com
1021-9986/2020/2/263-272 10/$/6.00

micropolar fluid in a trapezoidal cavity has been presented by *Gibanovet al.* [3]. The bottom wall of the cavity was kept at high constant temperature, whereas the inclined walls were at low temperatures while the top horizontal wall was adiabatic. It has been shown that an increase in the vortex viscosity parameter led to attenuation of the convective flow and heat transfer inside the cavity. Flow of micropolar fluid past a permeable stretching sheet in the presence of joule heating, thermal radiation, partial slip and Magneto HydroDynamic (MHD) with convective boundary conditions, was investigated by *Ramzan et al.* [4]. It was noted that the velocity and micro-rotation profiles decreased with an increase in the value of slip parameter. However, increase in the temperature distribution was seen with gradual mounting values of thermal radiation parameter. A comprehensive numerical study has been presented by *Akhter et al.* [5] for investigating the MHD flow and heat transfer characteristics of non-Newtonian micropolar fluid through a porous medium between two stretchable porous disks. *Hsiao* [6] investigated an applied thermal system for heat and mass transfer of hydromagnetic flow of micropolar nanofluids towards a stretching sheet with magnetic and viscous dissipation effects. The numerical results indicated that, compared to the magnetic field parameter, the material parameter had the opposite effect on the velocities, temperature, concentration, shear stress, Nusselt number and Schmidt number. *Habibi et al.* [7] investigated the buoyancy-driven boundary layer flow from a heated horizontal circular cylinder. Exact analytic solutions of the problem were obtained by employing the Optimal Homotopy Analysis Method (OHAM). The accuracy and reliability of the results were verified by comparing them with experimental results available in the literature. *Abdulaziz et al.* [8] studied the fully developed natural convection of MHD micropolar fluid flow in two vertical porous plates. Similarly, *Noor et al.* [9] studied the micropolar nanofluid which has mixed convection boundary layer flow adjacent to the stagnation point along a vertical stretching sheet. It was observed that the slip velocity between the nanoparticles and the base fluid considerably affected the heat transfer enhancement due to the micropolar nanofluid.

Haq et al. [10] performed the numerical simulation of water based magnetic nanoparticles between two parallel disks. *Zheng et al.* [11] studied the radiative heat transfer and mixed convection in the micropolar slip flow along a vertical permeable plate. *Hung et al.* [12] investigated the combined convection of micropolar fluids in a vertical wavy channels, saturated by porous media, by employing a coordinate transformation scheme. *Hung et al.* [13] numerically studied the phenomena of transient heat transfer in a micropolar fluid through wavy channels with porous media. To study the heat transfer in a porous medium saturated by a micropolar fluid between two parallel permeable disks along with the uniform suction or injection, *Umavathi* and *Sheka* [14] introduced the method of differential transform. *Rashidi et al.* [15] used the homotopy analysis method to study the MHD mixed convective heat transfer for laminar, electrically conducting viscoelastic fluid flow in a permeable wedge with thermal radiation effects. By applying the shooting method, *Malik et al.* [16] investigated the two dimensional mixed convection flow of MHD Erying –Powell nanofluid over a stretching sheet. In order to study the flow of MHD Oldroyd-B fluid, *Abbasbandy et al.* [17] applied the Keller Box method. It was noted that, in Oldroyd-B fluid, the skin friction coefficient was larger than in the viscous fluid. *Erfani* and *Rashidi* [18] studied the thermal diffusion and diffusion thermo effects on combined mass and heat transfer in a steady MHD convective and slip flow over a rotating disk. *Cai et al.* [19] is a good source for detailed review on nanofluids. *Khidir* and *Sibanda* [20] studied the flow over a nonlinear stretching sheet in electrically conducting nanofluid, along with the viscous dissipation. *Khan et al.* [21] introduced the two dimensional convective boundary layer flows of Ag-water and Cu-water nano fluids over a permeable semi-infinite moving plate. Based on the Darcy-Brinkman- Forchheimer flow model, *Tian et al.* [22] described the viscous dissipation effects on the fully developed in a flat channel, filled with porous medium and saturated by power law fluid. Further, Azarkhalil and Keyyani [23] and *Izadkhah et al.* [24] are excellent resources for nanofluids.

To our best knowledge no researcher has yet considered the thermal behavior of micropolar fluids in a porous channel under an oscillatory pressure gradient. Therefore, in this paper, we consider the unsteady, laminar, incompressible, and two-dimensional flow of micropolar fluid in a channel having permeable walls, under the influence of an external oscillatory pressure gradient. We use the three step explicit Runge-Kutta method for the time integration whereas the spatial

discretization is performed by using the central difference approximations. Effects of the governing parameters on the flow, microrotation and heat transfer aspects of the problem are discussed.

THEORITICAL SECTION

Problem formulation

Consider the two dimensional, incompressible and laminar micropolar fluid through a porous medium inside a parallel plate channel with wall transpiration. In this paper, we have assumed that the flow is pulsatile, and is driven by a pressure gradient with steady and oscillatory components, whereas the wall transpiration is modeled by considering the injection at the lower channel wall and the suction at the upper one. Further, the two walls are considered to be located at y = ±d. The suitable coordinate system for our problem is Cartesian coordinate system.

The governing momentum and microrotation equations of the problem are:

$$\frac{\partial u}{\partial \tau} + v_0 \frac{\partial u}{\partial y} = -\frac{1}{\rho}\frac{\partial p}{\partial x} + \left(\frac{\mu+\kappa}{\rho}\right)\frac{\partial^2 u}{\partial y^2} + \frac{\kappa}{\rho}\frac{\partial \upsilon_3}{\partial y} - \frac{\upsilon_B}{k_p}u - bu^2, \tag{1}$$

$$\rho j\left(\frac{\partial \upsilon_3}{\partial t} + v_0 \frac{\partial \upsilon_3}{\partial y}\right) = \gamma \frac{\partial^2 \upsilon_3}{\partial y^2} - \kappa\left(\frac{\partial v}{\partial x} - \frac{\partial u}{\partial y}\right) - 2\kappa\upsilon_3, \tag{2}$$

Where u is the horizontal velocity component, v_0 is the wall transpiration velocity, ρ is the density, p is the pressure, υ_B is the kinematic viscosity, υ_3 is the microrotation, k_p is the permeability of the porous medium and b is the inertial drag coefficient related to the porous medium. It is worthy to mention that the Eq. (1) is a combination of the momentum equation of micropolar fluid and the Forchheimer law, last two terms are due to this law. *Eringen* and *Suhubi* [23] introduced the micropolar continuum followed by micropolar fluid models characterized by the couple stress and a nonsymmetrical stress tensor. The theory and its applications were later developed in [24] and [25]. This theory comprises two independent kinematic quantities: the velocity vector and the microrotation vector. Further details may be found in an excellent work by *Dedic et al. [26]*.

The governing equation for heat transfer is:

$$\frac{\partial T}{\partial \tau} + v_0 \frac{\partial T}{\partial y} = \alpha \frac{\partial^2 T}{\partial y^2} \tag{3}$$

where, α is the thermal diffusivity and T is the temperature of the fluid. In Eq. (3), the first and second derivative terms stand for thermal convection and diffusion respectively. Since the two channel walls are located at different temperature, therefore the diffusion has been taken into account. Initially, no wall transpiration effects (suction/ injection) are assumed at the channel walls. Therefore, linear variation of temperature across the channel is considered. After this, it is the imposition of suction/injection which is responsible for the change in temperature profile.

The boundary conditions (for $t > 0$) are:

$$\left.\begin{aligned} u = 0, T = T_1, \upsilon_3 = 0 \quad & \text{at} \quad y = -d \\ u = 0, T = T_2, \upsilon_3 = 0 \quad & \text{at} \quad y = d \end{aligned}\right\} \tag{4}$$

where T_1 , T_2 are the fixed temperatures at the lower and upper walls of the channel, respectively.

We define the following dimensionless parameters,

$$U = \frac{u}{v_0}, \xi = \frac{x}{d}, \eta = \frac{y}{d}, \; t = \frac{v_0}{d}\tau, \qquad P = \frac{p}{\rho v_0^2}, \theta = \frac{T - T_m}{T_2 - T_m}, \upsilon_3 = \frac{v_0}{d} g(\eta) \tag{5}$$

From Eqs. (1)-(3) and the above dimensionless parameters, we have the following resulting equations:

$$\frac{\partial U}{\partial t} + \frac{\partial U}{\partial \eta} = -\frac{\partial P}{\partial \xi} + \left(\frac{1+C_1}{R}\right)\frac{\partial^2 U}{\partial \eta^2} + \frac{C_1}{R}G'(\eta) - \frac{1}{\lambda}U - Nf\, U^2 \tag{6}$$

$$\frac{\partial G}{\partial t} + G' = C_3 G'' - C_1 C_2\left(\frac{\partial U}{\partial \eta} + 2G\right) \tag{7}$$

$$\frac{\partial \theta}{\partial t} + \frac{\partial \theta}{\partial \eta} = \frac{1}{R\,Pr}\frac{\partial^2 \theta}{\partial \eta^2} \tag{8}$$

Where $R = \frac{dv_0}{\upsilon_B}$ is the Reynolds number, $\lambda = \frac{k_p v_0}{d\upsilon_B}$ is the Darcy parameter, nf = db is the Forchheimer quadratic drag parameter, ($C_1 = \kappa/\mu$) is the vortex viscosity parameter, ($C_2 = d\mu / \rho j v_0$) is the microinertia density

Table 1: Dimensionless velocity U(η) on three grid sizes and extrapolated Values

U(η)				
η	1st grid (h = 0.02)	2nd grid (h = 0.01)	3rd grid (h = 0.005)	Extrapolated values
-0.8	0.447525	0.447484	0.447470	0.447466
-0.6	0.781962	0.781879	0.781851	0.781842
-0.4	1.014752	1.014633	1.014592	1.014578
-0.2	1.156062	1.155917	1.155867	1.155850
0	1.212317	1.212160	1.212106	1.212088
0.2	1.184260	1.184107	1.184055	1.184037
0.4	1.065715	1.065582	1.065537	1.065522
0.6	0.843191	0.843093	0.843060	0.843049
0.8	0.496435	0.496384	0.496366	0.496360

parameter, (C_3 = γ/ dρjv$_0$) is the spin gradient viscosity parameter and $\mathbf{Pr} = \frac{\upsilon_B}{\alpha}$ is the Prandtl number.

We defined the pressure gradient as:

$$-\frac{\partial \mathrm{P}}{\partial \xi} = \mathrm{Ps} + \mathrm{P0}\cos(\omega \mathrm{t}) \tag{9}$$

where *P0* is the static and *Ps* is the oscillatory components (with ω being its frequency) of the pressure gradient.

By using Eq. (4), the boundary conditions finally get the form,

$$\begin{aligned} &\eta = -1: \ \mathrm{U} = 0, \mathrm{G} = 0, \theta = -1, \\ &\eta = 1: \quad \mathrm{U} = 0, \mathrm{G} = 0, \ \theta = 1 \qquad \forall \ \mathrm{t} > 0 \end{aligned} \tag{10}$$

Initially, we assume that the fluid is at rest, and the temperature distributions vary linearly with η (that is, across the channel), which results in the following initial conditions:

$$\mathrm{U} = 0, \theta = \mathrm{G} = \eta \qquad \forall \ -1 \le \eta \le 1 \quad \text{at} \quad \mathrm{t} = 0 \tag{11}$$

Numerical solution

We have solved the Eqs. (6)-(8) subject to the initial and boundary conditions given in Eqs. (10) and (11) respectively, by employing the three step explicit Runge-Kutta method for time-integration whereas the spatial derivatives are approximated by the corresponding central differences.

RESULTS AND DISCUSSION

We numerically compute the velocity and temperature distributions across the channel for various values of the dimensionless parameters. The following values of the parameters are considered:

$$\begin{aligned} &\rho = 1050\,\mathrm{kg/m^3}, 2\mathrm{d} = 0.6\times10^{-2}\,\mathrm{m}, \\ &\mathrm{V_0} = 0.05\times10^{-2}\,\mathrm{m/s}, \mathrm{D} = 10^{-5}\,\mathrm{m^2/s}\ , \\ &\mu = 3.2\times10^{-3}\,\mathrm{N/sm^2}, \\ &\mathrm{c_p} = 14.286\,\mathrm{J/kg\,K}, \mathrm{k} = 2.2\times10^{-3}\,\mathrm{J/m\,s\,K}, \\ &\sigma = 0.8\mathrm{Sm^{-1}}, \mathrm{Pr} = 21, \mathrm{R} = 0.5, \ \omega = 8, \\ &\mathrm{P0} = 7, \mathrm{Ps} = 10, \lambda = 5, \mathrm{Nf} = 0.002, \\ &\mathrm{C_1} = 1, \mathrm{C_2} = 0.2 \,\text{and}\, \mathrm{C_3} = 0.3. \end{aligned}$$

Table 1 indicates that the convergence of our numerical results for *U(η)* with the above mentioned values of the governing parameters at t = 0.25, as the step-size *h* decreases. This gives us confidence on our numerical procedure. Different values of the micropolar parameters undertaken in the present study are given in the Table 2.

Physical model for the present problem is shown in the Fig. 1. On the other hand, Figs. 2 & 3 show the time variation of velocity and microrotation distribution across the channel. The number of cycles is controlled by the frequency parameter ω. It is noted that the peak value of the velocity in the first cycle is significantly lower than the ones corresponding to the next cycles. It is due to the reason that initially the fluid is at rest, and because of inertia, the pressure gradient (∂P/∂ξ) is not as effective as in the forthcoming cycles when the fluid is set in motion.

Table 2: Various cases of the micropolar parameters.

cases	C_1	C_2	C_3
1	0.0	0.0	0.0
2	0.5	0.1	0.2
3	1.0	0.3	0.5
4	1.5	0.7	0.8
5	2.0	1.0	1.2

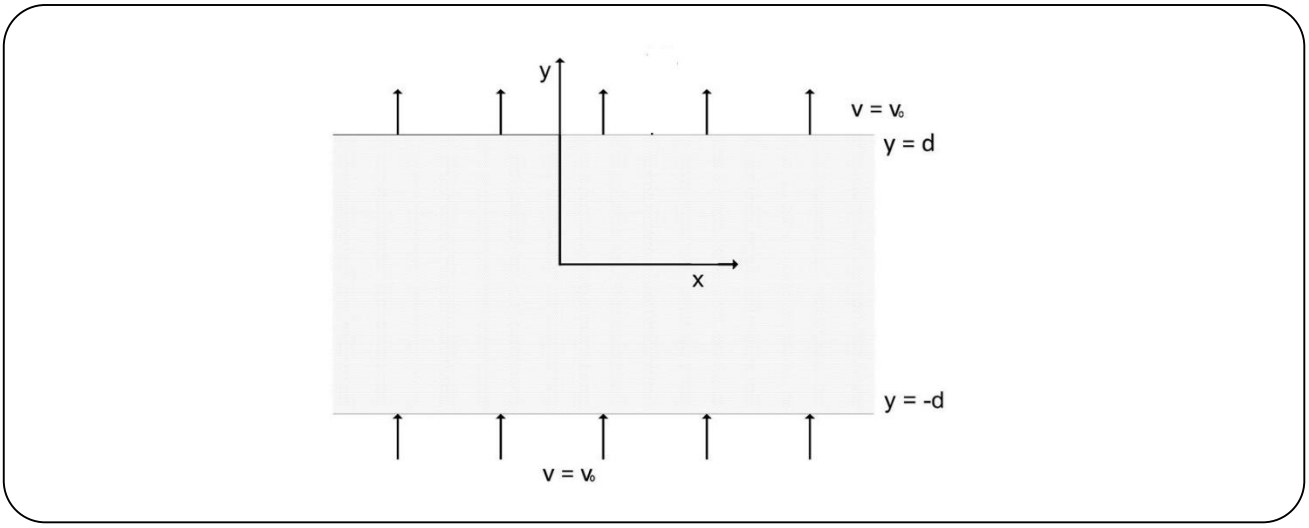

Fig. 1: Schematic diagram for the problem.

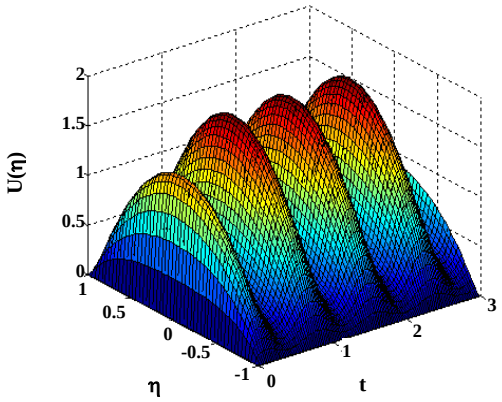

Fig. 2: Variation of velocity with time for R = 0.5, ω=8, P0 = 7, λ = 5, Nf = 0.002.

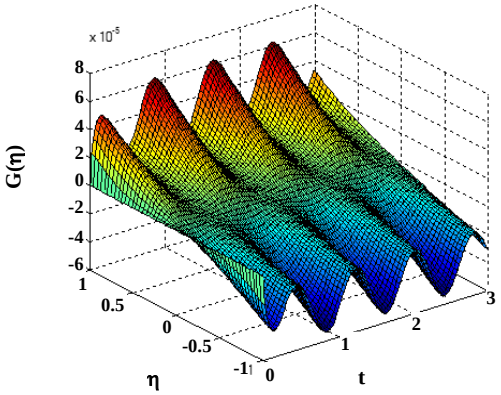

Fig. 3: Variation of microrotation with time for R = 0.5, ω = 8, Ps = 10, C_2 =0.2, C_3 = 0.3, P0 = 7, λ = 5, Nf = 0.002.

Figs. 4 & 5 demonstrate high velocity as well as the microrotation gradients near t = 0 on the application of pressure gradient to the stationary fluid. It may also be observed that cycles are elongated across the channel width and, after the first one, almost periodic. Figs. 6 & 7 illustrate the temperature distribution across the channel as the time passes. Initially, when the fluid is stagnant in the absence of any deriving force, the temperature is assumed

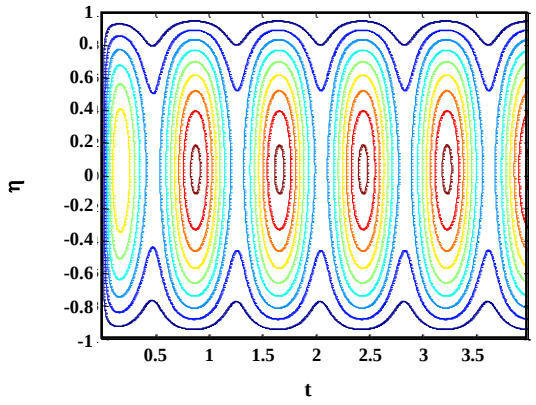

Fig. 4: Equi-velocity lines for R = 0.5, ω = 8, Ps = 10, C_1 = 1, C_2 0.2, C_3 = 0.3, P_0 = 7, λ = 5, Nf = 0.002.

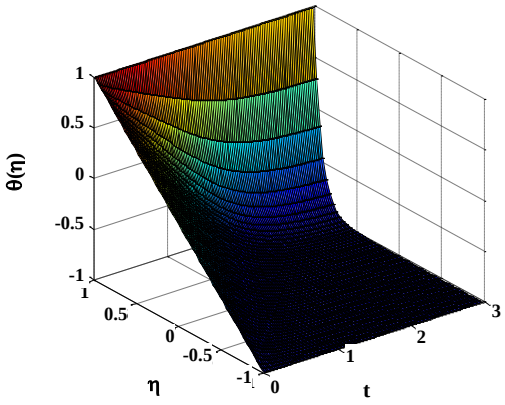

Fig. 6: Variation of temperature with time for R = 0.5, ω = 8, Ps = 10, C_1 = 1, C_2 = 0.2, C_3 = 0.3, P_0 = 7, λ = 5, Nf = 0.002.

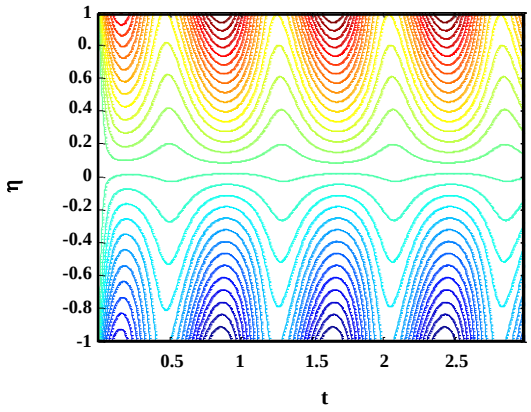

Fig. 5: Equi-microrotation lines for R = 0.5, ω = 8, P_0 = 7, λ = 5, Nf = 0.002.

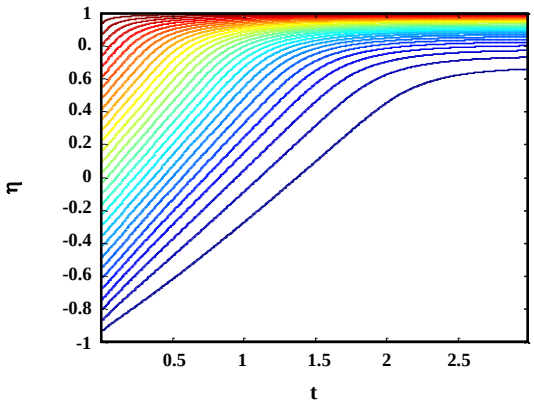

Fig. 7: Variation of microrotation with time for R = 0.5, ω = 8, Ps = 10, C_2 =0.2, C_3 = 0.3, P0 = 7, λ = 5, Nf = 0.002.

to be varying linearly across the channel. But once the fluid comes out of its stationary state, the temperature distribution is concentrated in a small portion towards the upper channel wall, and in the rest of the channel, the thermal profile is almost flat.

We now present the effect of the various parameters on the velocity, microrotation and temperature distribution at the arbitrary dimensionless time (say at t = 0.25).

Fig. 8 shows the effect of the transpiration Reynolds number on the velocity profiles. It is noted that, the effect of R is to accelerate the fluid across the channel. Furthermore, an increase in R would mean an increase in the suction velocity at the upper plate. Fig. 9 demonstrate that an increase in the Reynolds number tends to almost straighten the microrotation profile. Moreover, there is a small change (decreasing) in the temperature profiles Fig. 10. The influence of the microrotation parameter on the velocity distribution is qualitatively opposite to that of the Reynolds number while same effect for microrotation profiles, as shown in Figs. 11 &12.

The effect of the Darcy parameter λ is given in Fig. 13. An increase in λ would mean a reduction in the Darcian drag force (quantified by the term (-U / λ) in Eq. (6)). This would turn into decreasing the resistance to the flow and thus accelerating the micropolar fluid. Thus, the net effect of λ is to accelerate the fluid across the channel as given by the Fig. 13, whereas microrotation profiles fall at the lower wall and opposite effect at the other wall (see Fig. 14)

An increase in the Forchheimer quadratic drag parameter Nf would enhance the resistance to the flow

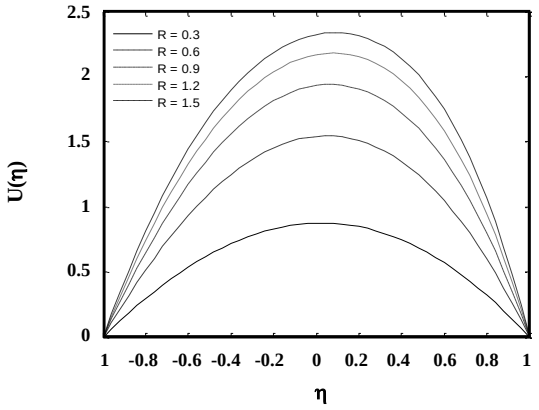

Fig. 8: Effect of the Reynolds number on the velocity profiles for ω = 8, Ps = 10, P0 = 7, λ = 5, C_1 = 1, C_2 = 0.2, C_3 = 0.3, Pr = 21, Nf = 0.002.

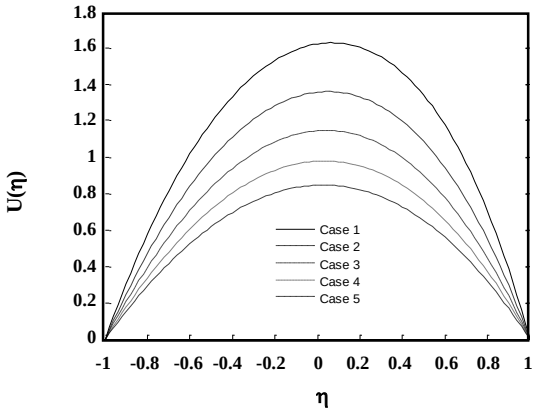

Fig. 11: Effect of the five cases of micropolar parameters on the velocity profiles for ω = 8, Ps = 10, P0 = 7, λ = 0.5, Pr = 2, Nf = 0.5.

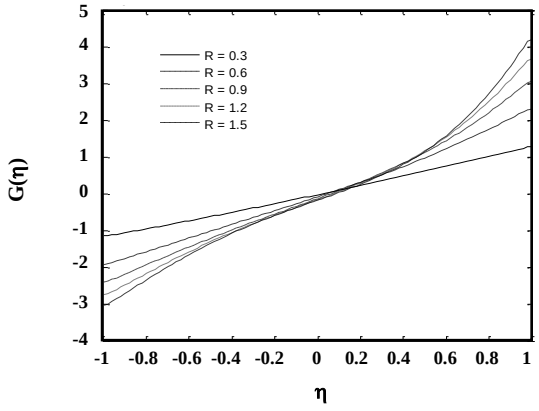

Fig. 9: Effect of the Reynolds number on the microrotation profiles for ω = 8, Ps = 10, P0 = 7, λ = 0.5, C_1 = 1, C_2 = 0.2, C_3 = 0.3, Pr = 2, Nf = 0.5.

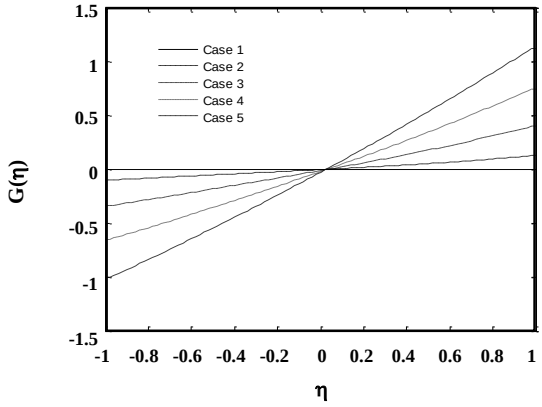

Fig. 12: Effect of the five cases of micropolar parameters on the microrotation profiles for ω = 8, Ps = 10, P0 = 7, λ = 0.5, Pr = 2, Nf = 0.5.

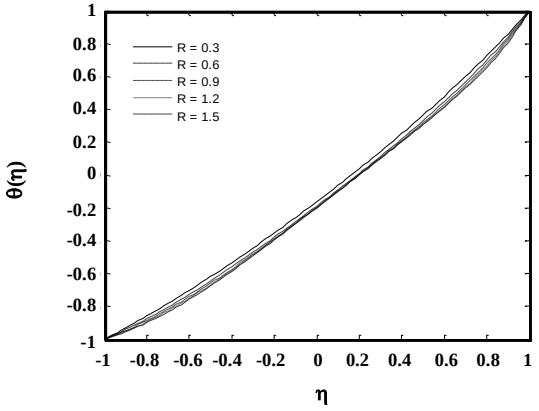

Fig. 10: Effect of the Reynolds number on the temperature profiles for ω = 8, Ps = 10, P0 = 7, λ = 0.5, C_1 = 1, C_2 = 0.2, C_3 = 0.3, Pr = 2, Nf = 0.5.

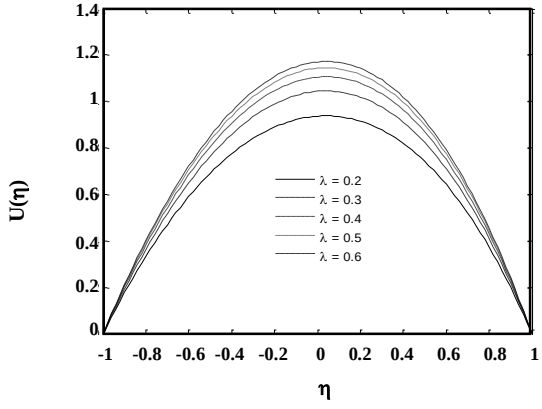

Fig. 13: Effect of the Darcy parameter on the velocity profiles for = 0.5, ω = 8, Ps = 10, P0 = 7, C_1 = 1, C_2 = 0.2, C_3 = 0.3 Pr = 2, Nf = 0.5.

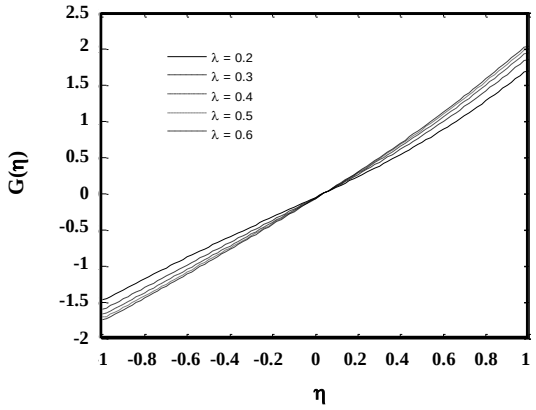

Fig. 14: Effect of the Darcy parameter on the microrotation profiles for R = 0.5, ω = 8, Ps = 10, P0 = 7, C_1 = 1, C_2 = 0.2, C_3 = 0.3, Pr = 2, Nf = 0.5.

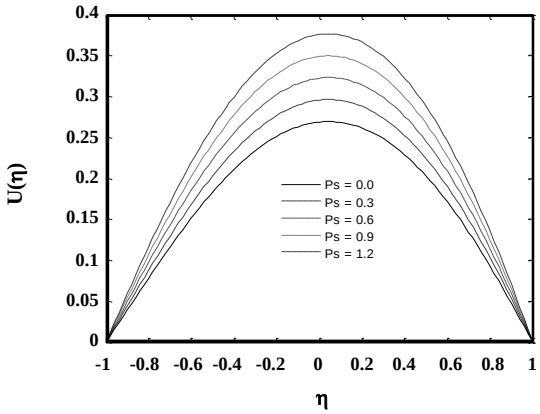

Fig. 17: Effect of the steady component of pressure gradient on the velocity profiles forR = 0.5, ω = 8, P0 = 7, λ = 0.5, C_1 = 1, C_2 = 0.2, C_3 = 0.3, Pr = 21, Nf = 0.5.

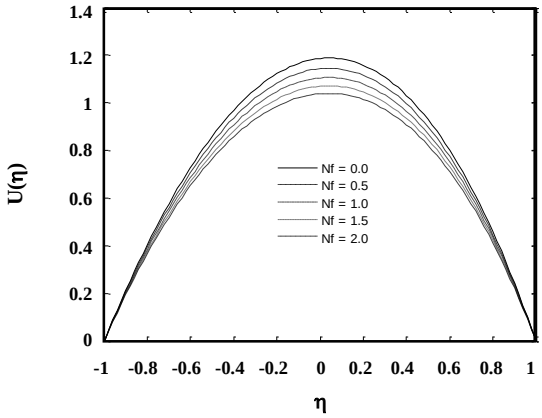

Fig. 15: Effect of the Forchheimer quadratic drag parameter on the velocity profiles for R = 0.5, ω = 8, Ps = 10, P0 = 7, λ = 0.5, C_1 = 1, C_2 = 0.2, C_3 = 0.3, Pr = 21.

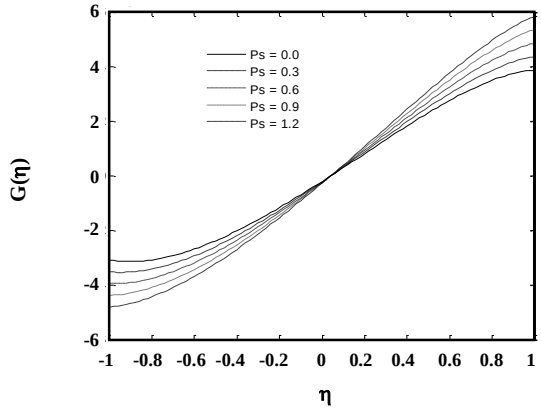

Fig. 18: Effect of the steady component of pressure gradient for R = 0.5, ω = 8, P0 = 7, λ = 0.5, C_1 = 1, C_2 = 0.2, C_3 = 0.3, Pr = 21, Nf = 0.5.

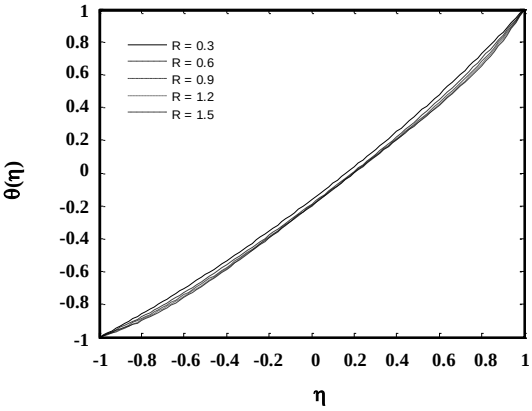

Fig. 16: Effect of the Forchheimer quadratic drag parameter on the microrotation profiles for R = 0.5, ω = 8, Ps = 10, P0 = 7, λ = 0.5, C_1 = 1, C_2 = 0.2, C_3 = 0.3, Pr = 21.

(characterized by the term $-NfU^2$ in Eq. (6)) and therefore will reduce the fluid velocity as shown in Fig. 15, while the effect of microrotation is same as that of Darcy parameter λ (see Fig. 16).

The effect of the steady component Ps of the pressure gradient is to remarkably accelerate the flow, whereas the effect on microrotation is opposite as that of Darcy parameter λ (please see Figs. 17 & 18).

It is note that, *P0* contributes to the oscillatory component of the driving force, and its influence on the velocity distribution depends on the sign of the term cos(ωt), at any instant of time. The effect of *P0* on the velocity and microrotation is same as that of Ps, as demonstrated in Figs. 19-20).

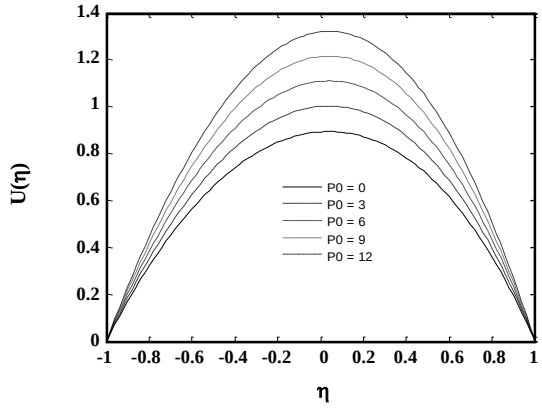

Fig. 19: Effect of the steady component of pressure gradient on the velocity profiles for R = 0.5, ω = 8, Ps = 10, C_1 = 1, C_2 = 0.2, C_3 = 0.3, Pr = 21, Nf = 0.5.

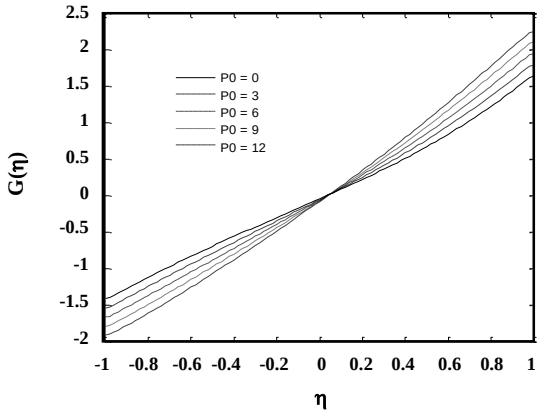

Fig. 20: Effect of the steady component of pressure gradient for R = 0.5, ω = 8, Ps = 10, λ = 0.5, C_1 = 1, C_2 = 0.2, C_3 = 0.3, Pr = 21, Nf = 0.5.

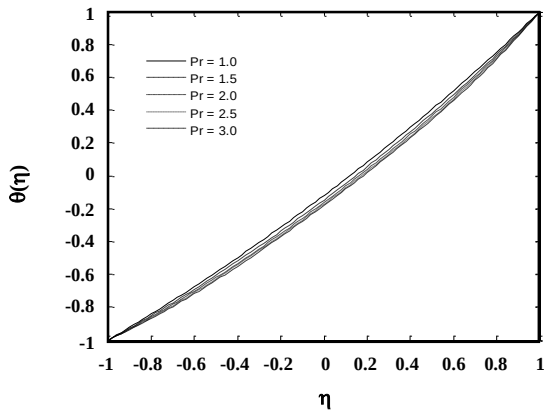

Fig. 21: Effects of the Prandtl number on the temperature profiles R = 0.3, ω = 8, P0 = 7, Ps = 10, λ = 0.5, C_1 = 1, C_2 = 0.2, C_3 = 0.3, Nf = 0.5.

Fig. 21 indicates how the thermal distribution across the channel is affected by the Prandtl number *Pr*. It is noted that an increase in *Pr* results in lowering the temperature profiles.

CONCLUSIONS

We have numerically studied the unsteady pulsatile micropolar fluid flow through a porous channel. Three step explicit Runge-Kutta method has been used for the time integration whereas the central difference approximations are employed for the spatial derivatives. It has been observed that the Reynolds number tends to accelerate the fluid across the channel, while flattening the temperature profiles. The Darcy parameter tends to accelerate the fluid, whereas the Forchheimer quadratic drag parameter and the magnetic parameter will reduce the fluid velocity. The effect of the steady component of the pressure gradient is to remarkably accelerate the flow whereas that of oscillatory component is time dependent. An increase in the Prandtl number tends to almost straighten the temperature profiles.

Acknowledgements:

The authors are extremely grateful to the learned reviewers for their useful comments to improve the quality of the manuscript.

Received : Apr. 7, 2018 ; Accepted : Jan. 23, 2019

REFERENCES

[1] Fakour M., Vahabzadeh A., Ganji D., Hatami M., Analytical Study of Micropolar Fluid Flow and Heat Transfer in a Channel with Permeable Walls, *Journal of Molecular Liquids*, **204**(3): 198-204 (2015).

[2] Mehrabian M.A., Kimiaeifar A., Golkarfard V., Akhgar A.R., Study of Chemically Reactive Flow and Heat Transfer in The Presence of a Uniform Magnetic Field, *Iran. J. Chem. Chem. Eng. (IJCCE)*, **35**: 119-137 (2016).

[3] Gibanov N.S., Sheremet M. A., Pop I., Free Convection in a Trapezoidal Cavity Filled with a Micropolar Fluid, *International Journal of Heat and Mass Transfer*, **99**: 831-838 (2016).

[4] Ramzan M., Farooq M., Hayat T., Chung J. D., Radiative and Joule Heating Effects in the MHD Flow of a Micropolar Fluid with Partial Slip and Convective Boundary Condition, *Journal of Molecular Liquids*, **221**: 394-400 (2016).

[5] Akhter S., Ashraf M., Ali K., MHD Flow and Heat Transfer Analysis of Micropolar Fluid Through a Porous Medium between Two Stretchable Disks Using Quasi-Linearization Method, *Iran. J. Chem. Chem. Eng. (IJCCE)*, **36**(4): 155-169 (2017).

[6] Hsiao K. L., Micropolar Nanofluid Flow with MHD and Viscous Dissipation Effects Towards a Stretching Sheet with Multimedia Feature, *International Journal of Heat and Mass Transfer*, **112**: 983-990 (2017)

[7] Habibi M. R., Amini M., Arefmanesh A., Ghasemikafrudi E., Effects of Viscosity Variations on Buoyancy-Driven Flow from a Horizontal Circular Cylinder Immersed in Al_2O_3-Water Nanofluid, *Iran. J. Chem. Chem. Eng. (IJCCE)*, **38**(1): 213-232 (2019)

[8]. Abdulaziz O., N. F M Noor N. F. M., Hashim I., Homotopy Analysis Method for Fully Developed MHD Micropolar Fluid Flow between Vertical Porous Plates, *Int. J. for Num Meth. Engin.*, **78**(7): 817-827 (2009).

[9] Noor N.F.M., Haq R.U., Nadeem S., Mixed Convection Stagnation Flow of a Micropolar Nanofluid Along a Vertically Stretching Surface with Slip Effects, *Meccanica*, **50**(8): 2007-2022 (2015).

[10] Haq U.R., Noor N.F.M., Khan Z.H., Numerical Simulation of Water Based Magnetic Nanoparticles between Two Parallel Disks, *Adv. Pow. Tech.*, **27**: 1568-1575 (2016).

[11] Zheng L., Liu N., Niu J., Zhang X., Slip and Buoyancy Lift Effects on the Mixed Convection Flow and Radiation Heat Transfer of a Micropolar Fluid Toward Vertical Permeable Plate, *J. of Por. Med.*, **16**: 575-583 (2013).

[12] Hung K.Y., Hsu T.H., Lin J.W., Mixed Convection of Micropolar Fluids in a Vertical Wavy Channel Saturated with Porous Media, *J. of Por. Med.*, **16**: 1107-1118 (2013).

[13] Hung K.Y., Hsu T. H., Lin J.W., Transient Behavior of Micropolar Fluids Through a Porous Wavy Channel, *J. of Por. Med.*, **17**: 1-15 (2014).

[14] Umavathi J., Sheka M., Flow and Heat Transfer in a Porous Medium Saturated by a Micropolar Fluid between Parallel Permeable Disks, *J. of Por. Med.*, **17**: 669-684 (2014).

[15] Rashidi M.M., Ali M., Freidoonimehr N., Rostami B., Hossain M.A., Mixed Convective Heat Transfer for MHD Viscoelastic Fluid Flow over a Porous Wedge with Thermal Radiation, *Int. J. of Ther. Sci.vol.* **2014**(87): 136-145 (2015).

[16] Malik M.Y., Khan I., Hussain A., Salahuddin T., Mixed Convection Flow of MHD Eyring-Powell Nanofluid over a Stretching Sheet: A numerical Study, *Amer. Inst. of Phy. AIP Adv.*, **5**, 117118 doi: 10.1063/1.4935639, (2015).

[17] Abbasbandy S., Hayat T., Alsaedi A., Rashidi M. M., Numerical and Analytical Solutions for Falkner-Skan Flow of MHD Oldroyd-B Fluid, *Int. J. of Num. Meth. for HFF*, **24**: 390-401 (2014).

[18] Rashidi M.M., Erfani E., Analytical Method for Solving Steady MHD Convective and Slip Flow Due to a Rotating Disk with Viscous Dissipation and Ohmic Heating, *Engine. Comput.*, **29**(6): 562-579 (2012).

[19] Cai J., Hu X., Xiao B., Zhou Y., Wei, W., Recent Developments on Fractal-Based Approaches to Nanofluids and Nanoparticle Aggregation, *Int. J. Heat Mass Transfer*, **105**: 623-637 (2017).

[20] Khidir A.A., Sibanda P., Nanofluid Flow over a Nonlinear Stretching Sheet in Porous Media with Mhd and Viscous Dissipation Effects, *J. of Por. Med.*, **17**: 391-403 (2014).

[21] Khan W.A., Uddin J.M., Ismail A.I. Md., Effect of Multiple Slips and Dissipation on Boundary Layer Flow of Nanofluid Flow over a Porous Flat Plate in Porous Media, *J. of Por. Med.*, **18**: 1-14 (2015).

[22] Tian X., Wang P., Xu S., Wu X, Comparison Study of Different Viscous Dissipation Effects on Forced Convection Heat Transfer in a Power Law Fluid Saturated Porous Medium, *J. of Por. Med.*, **19**: 885-900 (2016).

[23] Azarkhalil M.S., Keyyani B., Synthesis of Silver Nanoparticles from Spent X-Ray Photographic Solution via Chemical Reduction, *Iran. J. Chem. Chem. Eng. (IJCCE)*, **35**(3): 1-8 (2016).

[24] Izadkhah M., Erfan-Niya H., Moradkhani H., Rheological Behavior of Water-Ethylene Glycol Based Graphene Oxide Nanofluids, *Iran. J. Chem. Chem. Eng. (IJCCE)*, **37**(5): 177-187 (2018).